Chemical Physics Letters 696 (2018) 79–85

Contents lists available at ScienceDirect

Chemical Physics Letters

journal homepage: www.elsevier.com/locate/cplett

Research paper

Theoretical kinetics study of the reactions CHClBr + HBr ⇄ CH_2ClBr + Br, CCl_2Br + HBr ⇄ $CHCl_2Br$ + Br and $CClBr_2$ + HBr ⇄ $CHClBr_2$ + Br

Larisa L.B. Bracco *, María E. Tucceri, Carlos J. Cobos

Instituto de Investigaciones Fisicoquímicas Teóricas y Aplicadas (INIFTA), Departamento de Química, Facultad de Ciencias Exactas, Universidad Nacional de La Plata, CONICET, Casilla de Correo 16, Sucursal 4, La Plata 1900, Argentina

ARTICLE INFO

Article history:
Received 28 December 2017
In final form 13 February 2018
Available online 15 February 2018

Keywords:
CH_2ClBr, $CHCl_2Br$, $CHClBr_2$
H-atom abstractions by Br
Kinetics and quantum-chemical calculations

ABSTRACT

The kinetics of CHClBr + HBr ⇄ CH_2ClBr + Br (1, -1), CCl_2Br + HBr ⇄ $CHCl_2Br$ + Br (2, -2) and $CClBr_2$ + HBr ⇄ $CHClBr_2$ + Br (3, -3) reactions at 293–787 K has been studied by using the canonical transition state theory with molecular information provided by different quantum chemical methods. The obtained rate constants (in cm^3 $molecule^{-1}$ s^{-1}) are $k_1 = 5.24 \times 10^{-13}$ exp[−1.47 kcal mol^{-1}/RT], $k_{-1} = 2.70 \times 10^{-11}$ exp [−10.21 kcal mol^{-1}/RT], $k_2 = 4.18 \times 10^{-13}$ exp[−2.49 kcal mol^{-1}/RT], $k_{-2} = 6.96 \times 10^{-12}$ exp[−7.36 kcal mol^{-1}/RT], $k_3 = 3.29 \times 10^{-13}$ exp[−2.20 kcal mol^{-1}/RT], and $k_{-3} = 8.45 \times 10^{-13}$ exp[−7.10 kcal mol^{-1}/RT]. Rate constants for (2, -2) and (3, -3) are here reported for the first time.

1. Introduction

Through exchange processes with the atmosphere, oceans are a source of short lived bromocarbons like bromoform ($CHBr_3$), with an estimated atmospheric lifetime of 24 days [1], bromochloromethane (CH_2ClBr), bromodichloromethane ($CHBrCl_2$) and dibromochloromethane ($CHBr_2Cl$). Photolysis of bromocarbons elevates bromine concentrations and affects atmospheric chemistry [2]. Particularly, bromine influences the NO/NO_2 cycle and the lifetimes of other trace gases in the troposphere, and stimulates catalytic ozone depletion cycles in the stratosphere [3,4]. In the last years several investigation including experimental determinations, theoretical estimations and field campaigns, attempt to understand the role of the bromine species in atmospheric chemistry [5–7]. To evaluate the atmospheric impact of bromocarbons it is necessary to know their abundance and the reactions that occur with the different species present. In this way, it is required to determine the rate constants of processes in which bromine atoms and haloalkyl radicals are involved.

The purpose of this paper is to present a kinetics theoretical study of the following reactions:

$$CHClBr + HBr \rightleftarrows CH_2ClBr + Br \quad (1,-1)$$

$$CCl_2Br + HBr \rightleftarrows CHCl_2Br + Br \quad (2,-2)$$

$$CClBr_2 + HBr \rightleftarrows CHClBr_2 + Br \quad (3,-3)$$

The processes (1, -1) have been extensively investigated. The forward reaction (1) was experimentally studied over the range of 414–787 K in a heatable tubular reactor coupled to a photoionization mass spectrometer. The obtained rate constants were expressed as $k_1 = (4.9 \pm 1.1) \times 10^{-13}$ exp [−(1.96 ± 0.07) kcal mol^{-1}/RT] cm^3 $molecule^{-1}$ s^{-1} [8]. Two theoretical studies have been reported for this process. On one hand, Imrik et al. [9] derived the value of $k_1 = 2.67 \times 10^{-13}$ exp [−1.73 kcal mol^{-1}/RT] cm^3 $molecule^{-1}$ s^{-1} at 200–1000 K using the canonical variational transition state theory (CVTST) with small-curvature tunneling correction (SCT) combined with MP2/6-31G(d,p) calculations. On other hand, Zhang et al. [10] obtained the rate constant expression $k_1 = 5.97 \times 10^{-13}$ exp [−1.98 kcal mol^{-1}/RT] cm^3 $molecule^{-1}$ s^{-1} over the 200–4000 K range with the CTST corrected by tunneling effects and the CISD(T)/6-311 + G(3df,2p)//MP2/6-311 + G(d,p) approach.

Reaction (-1) was experimentally studied by Imrik et al. [9] using the laser flash photolysis technique coupled with Br atom resonance fluorescence detection and a relative-rate method with gas chromatographic analysis. The obtained results at 293–785 K were expressed as $k_{-1} = 4.55 \times 10^{-11}$ exp [−(11.39 ± 0.70) kcal mol^{-1}/RT] cm^3 $molecule^{-1}$ s^{-1}. Also Imrik et al. carried out a study of reaction (-1) at 200–1000 K using a theoretical methodology identical to the employed for reaction (1). The predicted rate constants were fitted with the Arrhenius expression $k_{-1} = 2.30 \times 10^{-11}$ exp [−13.07 kcal mol^{-1}/RT] cm^3 $molecule^{-1}$ s^{-1}. In addition, Seetula et al. [8] reported the values $k_{-1} = 2 \times 10^{-11}$ exp [−11.89 kcal mol^{-1}/RT] cm^3 $molecule^{-1}$ s^{-1}, obtained from transition state theory and MP2/6-31G(d,p) calculations. Finally, rate constants derived with the improved canonical variational transition state theory (ICVTST) with SCT corrections combined

* Corresponding author.
E-mail address: lbracco@inifta.unlp.edu.ar (L.L.B. Bracco).

https://doi.org/10.1016/j.cplett.2018.02.040
0009-2614/

with QCISD(T)/6-311 + G(3df,2p)//MP2/6-311 + G(d,p) calculations along the minimum energy path have been reported. The obtained rate constants between 200 and 4000 K are given by $k_{-1} = 4.79 \times 10^{-18}\ T^{2.25}\ \exp[-3980]/T\ cm^3\ molecule^{-1}\ s^{-1}$ [10].

To our knowledge reactions (2, -2) and (3, -3) have not been studied so far. In order to estimate their kinetic parameters for the first time, canonical transition state theory, (CTST) complemented with molecular information provided by different quantum chemical methods were employed in this investigation. To test the used methodology, reactions (1, -1) were also investigated and the corresponding results compared with the available kinetic information.

2. Computational methods

All quantum-chemical calculations were performed with the GAUSSIAN 09 program package [11]. The B3LYP [12–14], BMK [15], B98 [16], M06-2X [17], mPW2PLYP [18], hybrid formulations of the density functional theory (DFT) combined with the Pople's split-valence triple-zeta basis set 6-311++G(3df,3pd) were employed for the calculation of geometrical parameters (via analytic gradient methods) and harmonic vibrational frequencies (with analytical second order derivative methods). In addition, energy estimations were performed by using the high-level *ab initio* composite method G4 [19], combined with the aforementioned DFT models (G4//DFT). The harmonic frequencies derived with the pure G4 method (B3LYP/6-31G(2df,p)) were scaled by a factor of 0.9854 [19]. Transition state structures were located with Synchronous Transit-Guided Quasi-Newton (STQN) method and verified by intrinsic reaction coordinate (IRC) calculations at the BMK/6-311++G(3df,3pd) level of theory.

The kinetic calculations were performed using the canonical version of the transition state theory [20] with small curvature tunneling contributions (CTST/SCT) [21], with molecular information provided by the employed quantum chemical calculations. No commercial code was used to perform these kinetic calculations.

3. Results and discussion

3.1. Molecular parameters and harmonic vibrational frequencies

The structural parameters, harmonic vibrational frequencies and rotational constants for molecules, radicals and transition states involved in the studied reactions were obtained using the aforementioned DFT and the G4 *ab initio* model. The resultant parameters are listed in Tables S1–S6 of the Supplementary content, together with reported experimental values. The obtained bond lengths, bond angles, and vibrational frequencies for the halons CH_2ClBr, $CHCl_2Br$ and $CHClBr_2$ at the employed levels differ in only ±0.02 Å, ±1.2°, and ±15 cm^{-1}, respectively. A very good agreement between these and reported experimental and calculated values was also found [22–26]. The calculated structural parameters and vibrational frequencies for the radicals CHClBr, CCl_2Br and $CClBr_2$ differ in only ±0.03 Å, ±0.4°, and ±33 cm^{-1} at the employed levels of theory. These values are in very good agreement with the previous theoretical results [8,22,23,27].

3.2. Energetics

Table 1 shows the reaction enthalpies at 0 K (ΔH_r^0) for processes (1, -1), (2, -2) and (3, -3) calculated from the individual enthalpies at different levels of theory. In the cases where the G4 level was combined with molecular optimizations performed with the DFT methods, the corresponding enthalpies were calculated from the

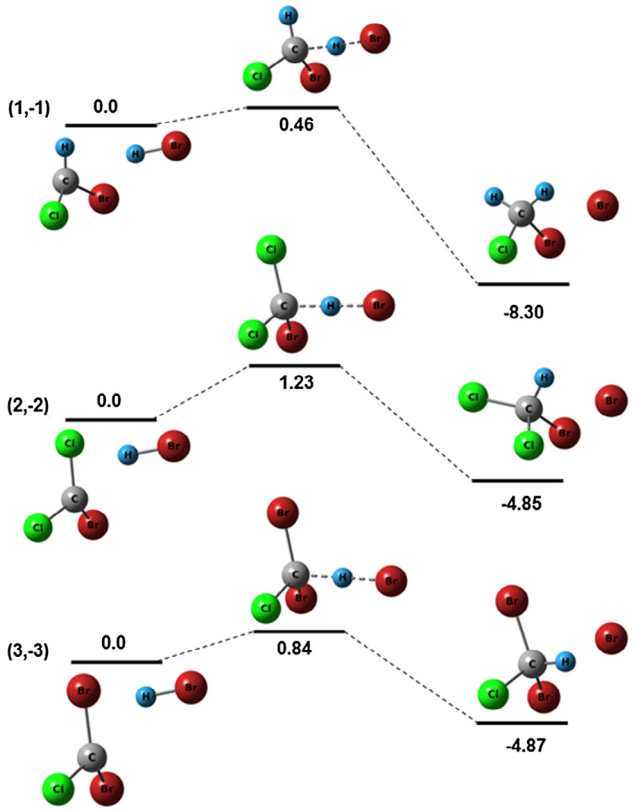

Fig. 1. Schematic diagram of the potential energy surface (in kcal mol^{-1}) for reactions (1,-1), (2,-2) and (3,-3) and geometrical structures calculated at the G4 level.

Table 1
Reaction enthalpies and enthalpy barriers at 0 K (in kcal mol^{-1}) for reactions (1,-1), (2,-2) and (3,-3).

	$CHClBr + HBr \rightleftarrows CH_2ClBr + Br$ (1, -1)			$CCl_2Br + HBr \rightleftarrows CHCl_2Br + Br$ (2, -2)			$CClBr_2 + HBr \rightleftarrows CHClBr_2 + Br$ (3,-3)		
Level of theory	ΔH_r^0	$\Delta H_{0,1}^{\#}$	$\Delta H_{0,-1}^{\#}$	ΔH_r^0	$\Delta H_{0,2}^{\#}$	$\Delta H_{0,-2}^{\#}$	ΔH_r^0	$\Delta H_{0,3}^{\#}$	$\Delta H_{0,-3}^{\#}$
B3LYP	−3.88	0.93	4.81	−0.21	2.77	2.98	−0.24	2.67	2.91
B98	−4.18	−0.37	3.81	−0.53	1.09	1.62	−0.40	1.06	1.46
BMK	−7.90	1.23	9.13	−4.46	2.59	7.05	−3.85	2.86	6.71
M062X	−8.78	−0.016	8.76	−5.50	0.43	5.93	−5.49	0.82	6.31
mPW2PLYP	−5.41	0.57	5.98	−2.09	2.05	4.14	−2.08	1.91	3.99
G4	−8.30	0.46	8.76	−4.85	1.23	6.08	−4.87	0.84	5.71
G4//B3LYP	−8.06	0.75	8.81	−4.31	1.45	5.76	−4.64	0.99	5.63
G4//B98	−8.16	0.60	8.76	−4.73	1.34	6.07	−4.74	0.93	5.67
G4//BMK	−8.24	0.37	8.61	−4.74	1.10	5.84	−4.49	0.89	5.38
G4//M062X	−8.11	0.67	8.78	−4.81	1.36	6.17	−4.63	0.92	5.72
G4//mPW2PLYP	−8.09	0.61	8.70	−4.82	1.27	6.09	−4.66	0.94	5.60

Table 2
Rate constants with tunneling corrections k (in cm^3 $molecule^{-1}$ s^{-1}), pre-exponential factors A (in cm^3 $molecule^{-1}$ s^{-1}) and activation energies E_a (in kcal mol^{-1}) for reactions (1, -1). Available experimental and theoretical determinations are included.

k_1 $CHClBr + HBr \rightarrow CH_2ClBr + Br$ (1)

T	G4	G4//B3LYP	G4//B98	G4//mPW2PLYP	G4//BMK	G4//M062X	Average	Average (E_a Corrected)	Exp. [8]	Calc. [10]	Calc. [9]
414	7.99×10^{-14}	1.28×10^{-13}	6.24×10^{-14}	6.35×10^{-14}	1.11×10^{-13}	1.15×10^{-13}	9.33×10^{-14}	4.84×10^{-14}	4.52×10^{-14}	5.38×10^{-14}	3.28×10^{-14}
450	8.81×10^{-14}	1.33×10^{-13}	6.96×10^{-14}	7.10×10^{-14}	1.18×10^{-13}	1.28×10^{-13}	1.01×10^{-13}	5.85×10^{-14}	5.47×10^{-14}	6.52×10^{-14}	3.96×10^{-14}
500	1.00×10^{-13}	1.43×10^{-13}	8.02×10^{-14}	8.02×10^{-14}	1.39×10^{-13}	1.49×10^{-13}	1.15×10^{-13}	7.29×10^{-14}	6.81×10^{-14}	8.14×10^{-14}	4.68×10^{-14}
550	1.14×10^{-13}	1.55×10^{-13}	9.21×10^{-14}	9.66×10^{-14}	1.57×10^{-13}	1.68×10^{-13}	1.30×10^{-13}	8.72×10^{-14}	8.15×10^{-14}	9.75×10^{-14}	5.48×10^{-14}
600	1.28×10^{-13}	1.68×10^{-13}	1.04×10^{-13}	1.05×10^{-13}	1.72×10^{-13}	1.94×10^{-13}	1.45×10^{-13}	1.01×10^{-13}	9.47×10^{-14}	1.13×10^{-13}	6.26×10^{-14}
650	1.46×10^{-13}	1.83×10^{-13}	1.10×10^{-13}	1.18×10^{-13}	1.99×10^{-13}	2.20×10^{-13}	1.63×10^{-13}	1.15×10^{-13}	1.07×10^{-13}	1.29×10^{-13}	7.0×10^{-14}
700	1.64×10^{-13}	1.99×10^{-13}	1.33×10^{-13}	1.34×10^{-13}	2.19×10^{-13}	2.50×10^{-13}	1.83×10^{-13}	1.28×10^{-13}	1.20×10^{-13}	1.44×10^{-13}	7.70×10^{-14}
787	1.99×10^{-13}	2.32×10^{-13}	1.64×10^{-13}	1.64×10^{-13}	2.72×10^{-13}	3.04×10^{-13}	2.22×10^{-13}	1.50×10^{-13}	1.40×10^{-13}	1.68×10^{-13}	8.83×10^{-14}
Arrhenius parameters											
A	4.96×10^{-13}	4.07×10^{-13}	4.13×10^{-13}	4.23×10^{-13}	6.58×10^{-13}	8.15×10^{-13}	5.24×10^{-13}	5.24×10^{-13}	4.9×10^{-13}	5.97×10^{-13}	2.67×10^{-13}
Ea	1.46	1.00	1.60	1.60	1.52	1.66	1.47	1.96	1.96	1.98	1.73

k_{-1} $CH_2ClBr + Br \rightarrow CHClBr + HBr$ (-1)

T	G4	G4/B3LYP	G4/B98	G4/mPW2PLYP	G4/BMK	G4/M062X	Average	Average (E_a corrected)	Exp. [9]	Calc. [10]	Calc. [9]	Calc. [8]
293	7.34×10^{-19}	6.61×10^{-19}	3.46×10^{-19}	8.22×10^{-19}	1.35×10^{-18}	7.07×10^{-19}	7.70×10^{-19}	2.82×10^{-19}	1.48×10^{-19}	2.19×10^{-18}	2.16×10^{-21}	2.71×10^{-20}
350	1.08×10^{-17}	9.60×10^{-18}	5.06×10^{-18}	1.15×10^{-17}	1.85×10^{-17}	1.02×10^{-17}	1.09×10^{-17}	5.62×10^{-18}	3.59×10^{-18}	2.78×10^{-17}	5.60×10^{-20}	7.53×10^{-19}
450	2.61×10^{-16}	2.45×10^{-16}	1.22×10^{-16}	3.18×10^{-16}	4.22×10^{-16}	2.46×10^{-16}	2.69×10^{-16}	1.72×10^{-16}	1.37×10^{-16}	5.04×10^{-16}	2.31×10^{-18}	3.36×10^{-17}
500	8.35×10^{-16}	7.39×10^{-16}	3.89×10^{-16}	8.35×10^{-16}	1.32×10^{-15}	7.81×10^{-16}	8.16×10^{-16}	5.68×10^{-16}	4.89×10^{-16}	1.39×10^{-15}	8.50×10^{-18}	1.27×10^{-16}
550	2.22×10^{-15}	1.95×10^{-15}	1.03×10^{-15}	2.18×10^{-15}	3.46×10^{-15}	2.06×10^{-15}	2.15×10^{-15}	1.51×10^{-15}	1.38×10^{-15}	3.18×10^{-15}	2.46×10^{-17}	3.77×10^{-16}
600	5.09×10^{-15}	4.49×10^{-15}	2.35×10^{-15}	5.01×10^{-15}	7.87×10^{-15}	4.73×10^{-15}	4.92×10^{-15}	3.42×10^{-15}	3.30×10^{-15}	6.36×10^{-15}	5.99×10^{-17}	9.34×10^{-16}
650	1.04×10^{-14}	9.24×10^{-15}	4.82×10^{-15}	1.02×10^{-14}	1.61×10^{-14}	9.69×10^{-15}	1.01×10^{-14}	6.02×10^{-15}	6.88×10^{-15}	1.14×10^{-14}	1.27×10^{-16}	2.01×10^{-15}
700	1.99×10^{-14}	1.74×10^{-14}	9.06×10^{-15}	1.93×10^{-14}	3.00×10^{-14}	1.82×10^{-14}	1.90×10^{-14}	1.23×10^{-14}	1.29×10^{-14}	1.89×10^{-14}	2.41×10^{-16}	3.88×10^{-15}
785	4.92×10^{-14}	4.36×10^{-14}	2.26×10^{-14}	4.80×10^{-14}	7.46×10^{-14}	4.55×10^{-14}	4.72×10^{-14}	2.83×10^{-14}	3.14×10^{-14}	3.82×10^{-14}	5.98×10^{-16}	9.79×10^{-15}
Arrhenius parameters												
A	2.98×10^{-11}	2.60×10^{-11}	1.35×10^{-11}	2.63×10^{-11}	3.97×10^{-11}	2.68×10^{-11}	2.70×10^{-11}	2.70×10^{-11}	4.65×10^{-11}	1.28×10^{-11}	1.04×10^{-12}	2.00×10^{-11}
Ea	10.29	10.27	10.26	10.14	10.11	10.25	10.21	10.70	11.39	9.07	11.64	11.89

G4 total electronic energy considering the zero-point energies corrections from the corresponding DFT methods. All the reactions present electronic energy barriers connecting the reactants with products, whose computed values at 0 K, $\Delta H_0^{\#}$, are given also in Table 1. A standard normal-mode-analysis indicates that all obtained transition state structures have only one imaginary frequency and confirms the presence of true transitions states. The connectivity between the reactants, transition states and products was verified by IRC calculations at the BMK/6-311++G(3df,3pd) level (see Fig. S1 of Supplementary content). The G4 and the G4//DFT calculations predict transition states located at about 0.6, 1.3 and 0.9 kcal mol^{-1} above the reactants for reactions (1), (2) and (3), respectively. On the other side, reactions (-1), (-2) and (-3) present higher enthalpy barriers, being the corresponding average values of about 8.7, 6.0 and 5.6 kcal mol^{-1}, respectively. The transition state structures obtained with the different quantum-chemical methods are very similar. Geometrical parameters, harmonic vibrational frequencies and rotational constants for the transitions states are listed in Tables S3 and S6 of the Supplementary content. They present elongated C-H and H-Br bonds respect to the corresponding halon and HBr, respectively. The transition state structures calculated here for reactions (1) and (-1) are similar to those reported by Imrik et al. [9], Zhang et al. [10] and Seetula et al. [8] with the (R-U)MP2 (full)/6-31G(d,p), MP2/6-311+G(d,p) and MP2/6-31G(d,p) methods, respectively. Fig. 1 shows the schematic diagram of the potential energy surface for the studied reactions at the G4 level together with the optimized species involved. In general, similar reaction enthalpies and enthalpy barriers were obtained at the G4, G4//B3LYP, G4//B98, G4//mPW2PLYP, G4//BMK and G4//M062X levels of theory. Particularly, the results for reactions (1) and (-1) are in reasonable agreement with the values derived by Seetula et al. [27]. The calculations using DFT methods led to more dispersed result. Particularly, the B3LYP, B98 and mPW2PLYP conduce to smaller reactions enthalpies and electronic barriers than the G4, G4//DFT, M06-2X and BMK methods. Although the DFT describe very well the geometry of the species involved, not all of them are efficient to describe the reaction energetic. For that reason, the *ab initio* G4 method and its combinations with the geometry obtained with DFT were selected to evaluate the reaction rate constants.

Other possible reaction channels for the halon + Br reactions were also investigated. Particularly, the energetic of the Cl- and Br- abstractions processes were calculated with the G4 model. The resulting ΔH_r^0 values are presented in Table S7 of supplementary content. These results show that the Cl- and Br- abstractions by Br atom are more than 14 kcal mol^{-1} endothermic than reactions (-1), (-2) and (-3) and, in consequence, they are not competitive channels.

3.3. Kinetic analysis

To find the theoretical methods which better describe the available experimental information [8,9], the rate constants for reactions (1) and (-1) were estimated at different levels of theory. Then, using this methodology, rate constants for reactions (2, -2) and (3, -3) were predicted. For that purpose, canonical transition state theory [20] with small curvature tunneling contributions (CTST/SCT) were employed [21]. The selected temperature range, 293–787 K, include the available experimental data.

The corresponding rotational and vibrational partition functions for the reagents and transition states were calculated within the rotor/harmonic oscillator approximation, and they were evaluated using the molecular input data obtained from the quantum-chemical calculations listed in Tables S1–S6 of Supplementary content. The calculated CTST rate constants for reaction (-1) were multiplied by a factor of 2 to consider the 2 possible H-abstractions pathways [28,29]. The resulting rate constants k, pre-exponential factors A and activation energies E_a for reactions (1) and (-1) with tunneling correction are listed in Table 2 and without tunneling correction in Table S8. As can be seen, similar values were obtained with the G4 and G4//DFT composite models. In order to make comparisons, Tables 2 and S8 also include averaged values derived from the individual rate constants values together with previous experimental and theoretical results. As it can be observed, at the temperatures studied, the contributions by tunnel effect are small (see Table S8 of the Supplementary material). In fact, between 414 and 787 K the tunneling corrected rate constants are only 1.05–1.01 larger than the uncorrected rate constants. In addition, our rate constants are 2.1–1.5 times larger than those measured by Seetula et al. [8]. However, they can be satisfactorily matched by adding 0.49 kcal mol^{-1} to the averaged activation energy of 1.47 kcal mol^{-1}. In Fig. 2, an Arrhenius plot for reaction (1) is shown. The average corrected rate constants computed with tunneling corrections from this work (points) and the corresponding linear fits (lines) together with values from previous investigations are given, in all the cases the R^2 values are close to 1. As can be seen, the small electronic barrier in reaction (1) can be significantly affected by the errors in the calculations, and the small correction of 0.49 kcal mol^{-1} in the activation energy of reaction (1) is smaller than the normal uncertainty in the high-level of theory calculations. In fact, the mean unsigned deviation resulting from an analysis of well-known 76 barriers heights is for the G4 model of 1.36 kcal mol^{-1} [30]. Smaller errors are expected when more accurate

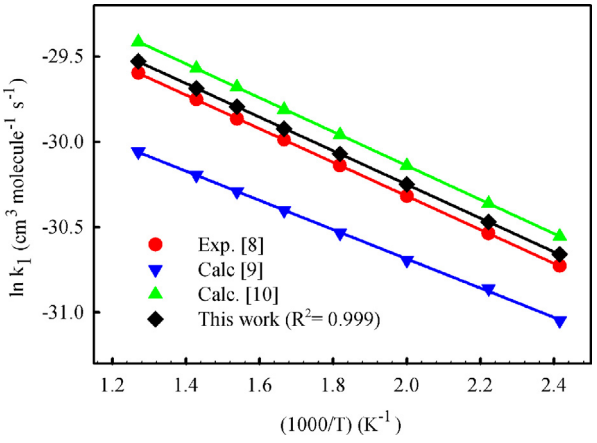

Fig. 2. Arrhenius plot for reaction (1).

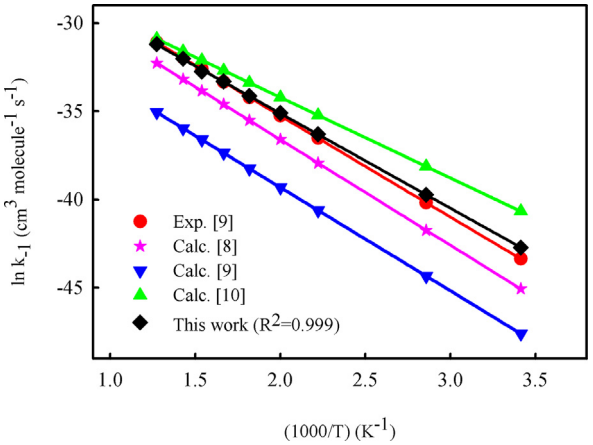

Fig. 3. Arrhenius plot for reaction (-1).

transition state geometries are employed [30]. It is also observed from Fig. 2, than the theoretical determinations made by Zhang et al. [10] are in better agreement with the experimental values than the estimations of Imrik et al. [9].

Results corresponding to reaction (-1) with tunneling corrections are presented in Table 2 (the uncorrected rate constants are listed in Table S9 of Supplementary content) and in Fig. 3. As for reaction (1), the averaged values of the present study are a factor of 2 larger than the experimental ones at 450 K and a factor of 1.5 at 785 K. [9]. However, a better agreement is found if a similar correction of 0.49 kcal mol^{-1} to the averaged activation energies is realized. The rest theoretical results exhibit higher discrepancies when compared with the experimental values [9,10].

Fig. 4 shows the equilibrium constants for the process (1, -1) estimated as $K_C = k_1/k_{-1} = 1.94 \times 10^{-2}$ exp [8.74 kcal mol^{-1}/RT] using the averaged rate constants $k_1 = 5.24 \times 10^{-13}$ exp [−1.47 kcal mol^{-1}/RT)] cm^3 $molecule^{-1}$ s^{-1} and $k_{-1} = 2.70 \times 10^{-11}$ exp [−10.21 kcal mol^{-1}/RT] cm^3 $molecule^{-1}$ s^{-1}. The results are compared with the equilibrium constants calculated from the experimental k_1 and k_{-1} values determined by different experimental techniques [8,9]. Supporting our entropic and energetic results, there is a very good agreement between the experimental K_C values and the present determinations over the whole temperature range. On the other side, there are notorious differences between the experimental values and the results of Imrik et al. [9]. The data derived from Zhang et al. [10] are similar to the experimental ones at high temperatures but the agreement is worse at low temperatures.

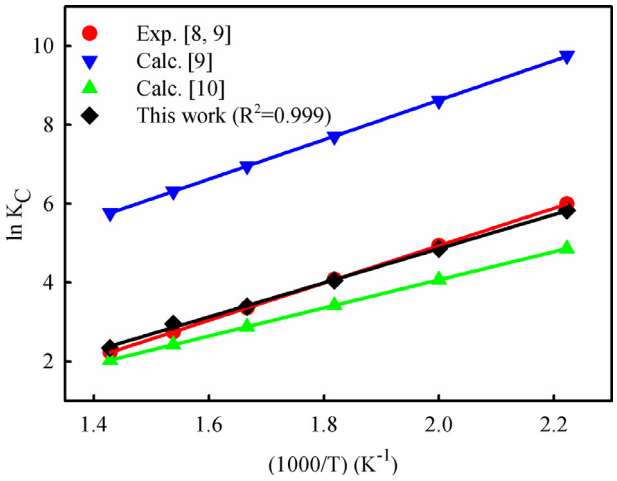

Fig. 4. Equilibrium constant for the process (1,-1) estimated from the respective averaged rate constants for reactions (1) and (-1). Available experimental and theoretical estimations are included.

In the absence of experimental and theoretical data, a study similar to the previous one was carried out to estimate the rate constants k_2, k_{-2}, k_3 and k_{-3}. In this way, canonical transition state theory [20] with small corrections due to tunnel effect (CTST/SCT) were employed [21], but in these cases, no correction was applied to the averaged activation energies because the value found for reaction (1) is not necessarily transferable to reactions (2) and (3). The employed molecular input data are given in Table 1 and in the Supplementary content (Tables S1–S6). The resulting rate constants are showed in Tables 3 and 4. The kinetic results without tunneling corrections are very similar and are presented in Tables S10 and S11 of the Supplementary content. As can be seen, similar results were obtained at the different levels of theory. Therefore, the average rate constants (in cm^3 $molecule^{-1}$ s^{-1}) k_2 and k_3 at 414–787 K, and k_{-2} and k_{-3} at 293–785 K can be recommended:

$$k_2 = 4.18 \times 10^{-13} \exp[-2.49 \text{ kcal mol}^{-1}/RT]$$

$$k_{-2} = 6.96 \times 10^{-12} \exp[-7.36 \text{ kcal mol}^{-1}/RT]$$

$$k_3 = 3.29 \times 10^{-13} \exp[-2.20 \text{ kcal mol}^{-1}/RT]$$

$$k_{-3} = 8.45 \times 10^{-13} \exp[-7.10 \text{ kcal mol}^{-1}/RT]$$

Table 3
Rate constants with tunneling correction k (cm^3 $molecule^{-1}$ s^{-1}), pre-exponential factors A (cm^3 $molecule^{-1}$ s^{-1}) and activation energies E_a (in kcal mol^{-1}) for reactions (2, -2).

T	G4	G4//B3LYP	G4//B98	G4//mPW2PLYP	G4//BMK	G4//M062X	Average
k_2 $CCl_2Br + HBr \rightarrow CHCl_2Br + Br$ (2)							
414	1.92×10^{-14}	1.46×10^{-14}	1.53×10^{-14}	2.03×10^{-14}	2.33×10^{-14}	3.88×10^{-14}	2.19×10^{-14}
450	2.28×10^{-14}	1.77×10^{-14}	1.85×10^{-14}	2.22×10^{-14}	2.73×10^{-14}	4.68×10^{-14}	2.59×10^{-14}
500	2.87×10^{-14}	2.23×10^{-14}	2.36×10^{-14}	2.73×10^{-14}	3.37×10^{-14}	5.94×10^{-14}	3.25×10^{-14}
550	3.54×10^{-14}	2.79×10^{-14}	2.94×10^{-14}	3.33×10^{-14}	4.09×10^{-14}	7.41×10^{-14}	4.02×10^{-14}
600	4.31×10^{-14}	3.43×10^{-14}	3.61×10^{-14}	4.00×10^{-14}	4.92×10^{-14}	9.12×10^{-14}	4.90×10^{-14}
650	5.18×10^{-14}	4.16×10^{-14}	4.37×10^{-14}	4.77×10^{-14}	5.85×10^{-14}	1.11×10^{-13}	5.90×10^{-14}
700	6.18×10^{-14}	4.99×10^{-14}	5.23×10^{-14}	5.64×10^{-14}	6.89×10^{-14}	1.33×10^{-13}	7.04×10^{-14}
787	8.20×10^{-14}	6.66×10^{-14}	6.98×10^{-14}	7.40×10^{-14}	9.01×10^{-14}	1.79×10^{-13}	9.36×10^{-14}
Arrhenius parameters							
A	3.66×10^{-13}	3.20×10^{-13}	3.36×10^{-13}	2.80×10^{-13}	3.60×10^{-13}	8.65×10^{-13}	4.18×10^{-13}
Ea	2.49	2.60	2.60	2.25	2.31	2.62	2.49
k_{-2} $CHCl_2Br + Br \rightarrow CCl_2Br + HBr$ (-2)							
293	2.79×10^{-17}	3.28×10^{-17}	1.61×10^{-17}	2.03×10^{-17}	2.92×10^{-17}	3.50×10^{-17}	2.69×10^{-17}
350	1.83×10^{-16}	1.87×10^{-16}	1.06×10^{-16}	1.23×10^{-16}	1.78×10^{-16}	2.30×10^{-16}	1.68×10^{-16}
450	1.82×10^{-15}	1.57×10^{-15}	1.03×10^{-15}	1.13×10^{-15}	1.60×10^{-15}	2.31×10^{-15}	1.58×10^{-15}
500	4.28×10^{-15}	3.49×10^{-15}	2.41×10^{-15}	2.58×10^{-15}	3.63×10^{-15}	5.49×10^{-15}	3.65×10^{-15}
550	8.85×10^{-15}	6.88×10^{-15}	4.94×10^{-15}	5.22×10^{-15}	7.31×10^{-15}	1.14×10^{-14}	7.43×10^{-15}
600	1.66×10^{-14}	1.24×10^{-14}	9.18×10^{-15}	9.60×10^{-15}	1.33×10^{-14}	2.16×10^{-14}	1.38×10^{-14}
650	2.86×10^{-14}	2.08×10^{-14}	1.58×10^{-14}	1.64×10^{-14}	2.27×10^{-14}	3.78×10^{-14}	2.37×10^{-14}
700	4.65×10^{-14}	3.28×10^{-14}	2.55×10^{-14}	2.63×10^{-14}	3.62×10^{-14}	6.19×10^{-14}	3.82×10^{-14}
785	9.47×10^{-14}	6.43×10^{-14}	5.13×10^{-14}	5.27×10^{-14}	7.21×10^{-14}	1.28×10^{-13}	7.72×10^{-14}
Arrhenius parameters							
A	9.53×10^{-12}	4.65×10^{-12}	5.01×10^{-12}	4.49×10^{-12}	5.97×10^{-12}	1.32×10^{-11}	6.96×10^{-12}
Ea	7.52	7.01	7.46	7.27	7.22	7.59	7.36

Table 4
Rate constants with tunneling correction k (cm^3 $molecule^{-1}$ s^{-1}), pre-exponential factors A (cm^3 $molecule^{-1}$ s^{-1}) and activation energies E_a (in kcal mol^{-1}) for reactions (3, -3).

T	G4	G4//B3LYP	G4//B98	G4//mPW2PLYP	G4//BMK	G4//M062X	Average
k_3 $CClBr_2 + HBr \rightarrow CHClBr_2 + Br$ (3)							
414	2.77×10^{-14}	2.37×10^{-14}	2.31×10^{-14}	2.48×10^{-14}	2.29×10^{-14}	2.37×10^{-14}	2.43×10^{-14}
450	3.21×10^{-14}	2.76×10^{-14}	2.70×10^{-14}	2.88×10^{-14}	2.65×10^{-14}	2.76×10^{-14}	2.83×10^{-14}
500	3.91×10^{-14}	3.37×10^{-14}	3.30×10^{-14}	3.48×10^{-14}	3.19×10^{-14}	3.38×10^{-14}	3.44×10^{-14}
550	4.70×10^{-14}	4.09×10^{-14}	3.98×10^{-14}	4.18×10^{-14}	3.81×10^{-14}	4.07×10^{-14}	4.14×10^{-14}
600	5.61×10^{-14}	4.89×10^{-14}	4.75×10^{-14}	4.96×10^{-14}	4.51×10^{-14}	4.85×10^{-14}	4.93×10^{-14}
650	6.62×10^{-14}	5.70×10^{-14}	5.64×10^{-14}	5.85×10^{-14}	5.29×10^{-14}	5.73×10^{-14}	5.80×10^{-14}
700	7.76×10^{-14}	6.83×10^{-14}	6.61×10^{-14}	6.84×10^{-14}	6.17×10^{-14}	6.70×10^{-14}	6.82×10^{-14}
787	1.01×10^{-13}	8.90×10^{-14}	8.57×10^{-14}	8.85×10^{-14}	7.92×10^{-14}	8.66×10^{-14}	8.83×10^{-14}
Arrhenius parameters							
A	3.77×10^{-13}	3.41×10^{-13}	3.28×10^{-13}	3.23×10^{-13}	2.80×10^{-13}	3.27×10^{-13}	3.29×10^{-13}
Ea	2.21	2.25	2.24	2.17	2.12	2.22	2.20
k_{-3} $CHCl_2Br + Br \rightarrow CCl_2Br + HBr$ (-3)							
293	4.44×10^{-17}	5.60×10^{-17}	2.79×10^{-17}	5.87×10^{-17}	7.72×10^{-17}	4.26×10^{-17}	5.11×10^{-17}
350	2.73×10^{-16}	3.26×10^{-16}	1.65×10^{-16}	3.38×10^{-16}	4.27×10^{-16}	2.67×10^{-16}	2.99×10^{-16}
450	2.49×10^{-15}	2.82×10^{-15}	1.46×10^{-15}	2.88×10^{-15}	3.46×10^{-15}	2.47×10^{-15}	2.60×10^{-15}
500	5.68×10^{-15}	6.32×10^{-15}	3.29×10^{-15}	6.41×10^{-15}	7.58×10^{-15}	5.66×10^{-15}	5.82×10^{-15}
550	1.15×10^{-14}	1.26×10^{-14}	6.52×10^{-15}	1.26×10^{-14}	1.48×10^{-14}	1.13×10^{-14}	1.15×10^{-14}
600	2.09×10^{-14}	2.27×10^{-14}	1.18×10^{-14}	2.28×10^{-14}	2.63×10^{-14}	2.10×10^{-14}	2.09×10^{-14}
650	3.55×10^{-14}	3.82×10^{-14}	1.98×10^{-14}	3.84×10^{-14}	4.34×10^{-14}	3.55×10^{-14}	3.51×10^{-14}
700	5.67×10^{-14}	6.06×10^{-14}	3.14×10^{-14}	6.07×10^{-14}	7.59×10^{-14}	5.67×10^{-14}	5.70×10^{-14}
785	1.12×10^{-13}	1.20×10^{-13}	6.22×10^{-14}	1.18×10^{-13}	1.31×10^{-13}	1.13×10^{-13}	1.09×10^{-13}
Arrhenius parameters							
A	9.56×10^{-12}	9.12×10^{-12}	4.88×10^{-12}	8.74×10^{-12}	9.2×10^{-12}	9.88×10^{-12}	8.45×10^{-12}
Ea	7.25	7.09	7.13	7.04	6.91	7.29	7.10

4. Conclusions

The quantum chemical and kinetic methodology applied in this work was tested with the available experimental rate data of reactions (1, -1) [8,9]. The obtained kinetic parameters for these processes are in better agreement with the experimental results than previous theoretical determinations [8–10]. Therefore, an identical procedure was employed to predict the same kinetic parameters for processes (2, -2) and (3, -3) for the first time.

Acknowledgements

This research project was supported by the Universidad Nacional de La Plata (11/X676), the Consejo Nacional de Investigaciones Científicas y Tecnicas CONICET (PIP 2012-134, PIP 2012-1134), and the Agencia Nacional de Promoción Científica y Tecnológica (PICT 2012-478).

Appendix A. Supplementary material

Supplementary data associated with this article can be found, in the online version, at https://doi.org/10.1016/j.cplett.2018.02.040.

References

[1] World Meteorological Organization, Global Ozone Research and Monitoring Project No. 52 Scientific Assesment of Ozone Depleton, Genova, Switzerland, 2010.
[2] S. Raimund, B. Quack, Y. Bozec, M. Vernet, V. Rossi, V. Garçon, Y. Morel, P. Morin, Sources of short-lived bromocarbons in the Iberian upwelling system, Biogeosciences 8 (2011) 1551–1564.
[3] R. von Glasow, R. von Kuhlmann, M.G. Lawrence, U. Platt, P.J. Crutzen, Impact of reactive bromine chemistry in the troposphere, Atmos. Chem. Phys. 4 (2004) 2481–2497.
[4] R.J. Salawitch, D.K. Weisenstein, L.J. Kovalenko, C.E. Sioris, P.O. Wennberg, K. Chance, M.K.W. Ko, C.A. McLinden, Sensitivity of ozone to bromine in the lower stratosphere, Geophys. Res. Lett. 32 (2005) L05811.
[5] A. Kerkweg, P. Jöckel, N. Warwick, S. Gebhardt, C.A.M. Brenninkmeijer, J. Lelieveld, Consistent simulation of bromine chemistry from the marine boundary layer to the stratosphere. Part 2: Bromocarbons, Atmos. Chem. Phys. 8 (2008) 5919–5939.
[6] R. Hossaini, H. Mantle, M.P. Chipperfield, S.A. Montzka, P. Hamer, F. Ziska, B. Quack, K. Krüger, S. Tegtmeier, E. Atlas, S. Sala, A. Engel, H. Bönisch, T. Keber, D. Oram, G. Mills, C. Ordóñez, A. Saiz-Lopez, N. Warwick, Q. Liang, W. Feng, F. Moore, B.R. Miller, V. Marécal, N.A.D. Richards, M. Dorf, K. Pfeilsticker, Evaluating global emission inventories of biogenic bromocarbons, Atmos. Chem. Phys. 13 (2013) 11819–11838.
[7] C.R. Thompson, P.B. Shepson, J. Liao, L.G. Huey, C. Cantrell, F. Flocke, J. Orlando, Bromine atom production and chain propagation during springtime Arctic ozone depletion events in Barrow, Alaska, Atmos. Chem. Phys. 17 (2017) 3401–3421.
[8] J.A. Seetula, Kinetics of the R+HBr⇄RH+Br (R=CH2Br, CHBrCl or CCl3) equilibrium. Thermochemistry of the CH2Br and CHBrCl radicals, Phys. Chem. Chem. Phys. 5 (2003) 849–855.
[9] K. Imrik, Gg. Kovács, I. Fejes, I. Szilágyi, D. Sarzyński, S. Dóbé, T. Bérces, F. Márta, J. Espinosa-García, Absolute and relative-rate kinetics experiments and direct dynamics computations for the reaction of Br atoms with CH2ClBr, J. Phys. Chem. A 110 (2006) 6821–6832.
[10] H. Zhang, B. Liu, L. Wang. X. Yu, Z. Li, J. Liu, C. Sun, Theoretical study on the reaction Br + CH2BrCl. Chem. Phys. 325 (2006) 531–537.
[11] M.J. Frisch et al., Gaussian Inc., Revision A.02, Wallingford, CT, USA, 2009.
[12] A.D. Becke, Density functional thermochemistry. III. The role of exact exchange, J. Chem. Phys. 98 (1993) 5648–5652.
[13] A.D. Becke, Density-functional exchange-energy approximation with correct asymptotic behavior, Phys. Rev. A 38 (1988) 3098–3100.
[14] C. Lee, W. Yang, R.G. Parr, Development of the Colle-Salvetti correlation-energy formula into a functional of the electron density, Phys. Rev. B 37 (1988) 785–789.
[15] A.D. Boese, J.M.L. Martin, Development of density functionals for thermochemical kinetics, J. Chem. Phys. 121 (2004) 3405–3416.
[16] H.L. Schmider, A.D. Becke, Optimized density functionals from the extended G2 test set, J. Chem. Phys. 108 (1998) 9624–9631.
[17] Y. Zhao, D.G. Truhlar, The M06 suite of density functionals for main group thermochemistry, thermochemical kinetics, noncovalent interactions, excited states, and transition elements: two new functionals and systematic testing of four M06-class functionals and 12 other functionals, Theor. Chem. Acc. 120 (2008) 215–241.
[18] T. Schwabe, S. Grimme, Towards chemical accuracy for the thermodynamics of large molecules: new hybrid density functionals including non-local correlation effects, Phys. Chem. Chem. Phys. 8 (2006) 4398–4401.
[19] L.A. Curtis, P.C. Redfern, K. Raghavachari, Gaussian-4 theory, J. Chem Phys. 126 (2007) 084108.
[20] S. Glasstone, K.J. Laidler, H. Eyring, The Theory of Rate Processes: The Kinetics of Chemical Reactions, Viscosity, Diffusion and Electrochemical Phenomena, McGraw-Hill Book Company Inc., New York, 1941.
[21] R.T. Skodje, D.G. Truhlar, Parabolic tunneling calculations, J. Phys. Chem. 85 (1981) 624–628.
[22] L.T. Areco Sánchez, PhD thesis, Facultad de Ciencias Exactas y Naturales, Universidad Nacional de Asunción, Paraguay, 2013.
[23] L.T. Areco Sanchez, L.L.B. Bracco, M.E. Tucceri, Theoretical estimation of enthalpies of formation of halons and related species, in preparation.

[24] S.A. Kudchadker, A.P. Kudchadker, Ideal gas thermodynamic properties of $CH_{4-(a+b+c+d)}F_aCl_bBr_cI_d$ Halomethanes, J. Phys Chem. Ref. Data 7 (4) (1978) 1285–1308.
[25] S. Giorgianni, B. De Carli, R. Visinoni, S. Ghersetti, Infrared spectrum and vibrational analysis of bromochloromethane, Spectrosc. Lett. 19 (1986) 1207–1214.
[26] S.R. Polo, A. Palm, F.L. Voelz, F.F. Cleveland, A.G. Meister, R.B. Bernstein, S.H. Sherman, Substituted Methanes. XXVI. Raman and infrared spectral data, assignments, potential constants, and thermodynamic properties for CHBrCl2 and CDBrCl2, J. Chem. Phys. 23 (1955) 833.
[27] J.A. Seetula, Ab initio study of the transition states for determining the enthalpies of formation of alkyl and halogenated alkyl free radicals, Phys. Chem. Chem. Phys. 2 (2000) 3807–3812.
[28] D.M. Bishop, K.J. Laidler, Symmetry numbers and statistical factors in rate theory, J. Chem. Phys. 42 (1965) 1688–1691.
[29] E. Pollak, P. Pechukas, Symmetry numbers, not statistical factors, should be used in absolute rate theory and in Broensted relations, J. Am. Chem. Soc. 100 (1978) 2984–2991.
[30] L.A. Curtiss, P.C. Redfern, K. Raghavachari, Assessment of Gaussian-4 theory for energy barriers, Chem. Phys. Lett. 499 (2010) 168–172.